IEEE Access
Multidisciplinary | Rapid Review | Open Access Journal

Received November 10, 2019, accepted November 27, 2019, date of publication December 2, 2019,
date of current version December 16, 2019.

Digital Object Identifier 10.1109/ACCESS.2019.2957103

An Improved Residual Chi-Square Test Fault Isolation Approach in Four-Gyro SINS

JIANHUA CHENG[1], XIANGYU SUN[1], PING LIU[1], AND HONGJIE MOU[2]
[1]College of Automation, Harbin Engineering University, Harbin 150001, China
[2]Shandong Institute of Space Electronic Technology, Yantai 264670, China

Corresponding author: Xiangyu Sun (sunxiangyu@hrbeu.edu.cn)

This work was supported in part by the National Nature Science Foundation of China under Grant 61633008, in part by the Heilongjiang Outstanding Youth Foundation under Grant JJ2018JQ0059, in part by the Fundamental Research Funds Central Universities under Grant HEUCFP201768, in part by the National Nature Science Foundation of China under Grant 61773132, and in part by the Seventh Generation Ultra Deep Water Drilling Unit Innovation Project.

ABSTRACT In this paper, an improved residual chi-square test fault isolation approach is proposed. In order to improve reliability of strapdown inertial navigation system (SINS), redundant SINS composed of redundant inertial sensors is applied. Among redundant SINS, four-gyro SINS has a wide range of applications as it supplies big reliability considering cost and volume. Fault isolation (FI) can isolate a fault when a fault occurs in redundant SINS. Generalized likelihood test (GLT) fault isolation based on kalman filter (KF) effectively isolate a fault because of its high sensitivity, small calculation and easy implementation. Nevertheless, GLT fault isolation based on KF cannot recognize a fault in four-gyro SINS. In this paper, first, a new observation model is introduced based on error models of a redundant SINS. In addition, a residual vector for isolation based on KF generated by gyros and star sensors is designed. Second, a separate residual chi-square test fault isolation approach for each gyro is proposed to recognize a fault. Third, an average separate residual vector and new isolation threshold are designed to reduce isolation time. At last, a star sensor is employed to obtain angular velocity, which provides angular velocity baseline information for the proposed isolation approach. Simulation shows that the proposed approach is useful to recognize a fault in four-gyro SINS.

INDEX TERMS SINS, FI, GLT, residual chi-square test, KF, reliability.

I. INTRODUCTION

As the most common navigation system, SINS can provide attitude, velocity and position of a vehicle, such as a ship, a spacecraft and an aircraft [1]. To get correct navigation information, high reliability of SINS is needed. However, SINS suffers a lot due to poor working environment or improper operation. In consequence, high reliability of SINS cannot be guaranteed all the time [2].

Among all components of SINS, inertial sensors (including gyros and accelerometers) are the most critical and easily damaged components [3]. As a result, redundant SINS is developed to increase reliability of SINS, which is obtained by utilizing multiple inertial sensors in SINS [4]. In redundant SINS, four-gyro SINS has a wide range of application as it supplies big reliability considering cost and volume [5], [6].

The associate editor coordinating the review of this manuscript and approving it for publication was Xiao-Sheng Si.

In four-gyro SINS, navigation result can be calculated from eight inertial sensors' outputs. Incorrect navigation results will be obtained if any one of the gyros or accelerometers fails. The International Federation of Automatic Control (IFAC) Safe Process Technical Committee defines a fault as an unpermitted deviation of at least one characteristic property or parameter of the system from the acceptable/usual/standard condition [7]. There are two ways to describe a fault: hard fault and soft fault. Hard faults present a sudden change on the basis of the normal outputs of sensors. Hard faults generally result from hardware damage, and make sensors fail immediately. Soft faults present a slow change on the basis of the normal outputs of sensors. Soft faults generally result from complex reasons, and cannot be detected immediately [7], [8].

FI is necessary when a fault occurs in four-gyro SINS. FI is to determine which sensor has a fault and judge the fault's type in redundant SINS. Current FI approaches are mainly for single fault. There are three kinds of FI approaches

for redundant SINS: direct comparison approach, signal processing approach and parity space approach. Direct comparison approach isolates a fault through linear relationship of multiple sensors. However, in four-gyro SINS, there is only one group of linear FI equation, and no FI truth table can be built up. As a result, direct comparison approach cannot isolate a fault in four-gyro SINS [9]–[11]. In addition, direct comparison approach cannot be applied when considering errors of inertial sensors.

Signal processing approach, such as linear estimation approach [12], variance identification approach [13] and wavelet transform approach [14], [15], can be applied to FI in four-gyro SINS. While they are only useful to a hard fault. Moreover, they show bad isolation performance when SINS change its motion state. Yan proposed mean test approach [16] to isolate a fault by testing mean value of an inertial sensor. However, the isolation results is not correct when considering errors of inertial sensors. In general, signal processing approach are all especially suitable for a hard fault, and they lose effectiveness when a soft fault happens.

Parity space approach, such as local estimation approach, optimal parity vector (OPT) approach, singular value decomposition (SVD) approach and GLT, is the most popular FI approach. They are useful when there is a hard fault or a soft fault. Local estimation approach can detect and isolate a small fault, but its amount of calculation is large, and it cannot diagnose a fault in time [17]. OPT has good robustness, but the rate of correct isolation is lower than that of correct detection [18], [19]. SVD cannot diagnose a fault with an opposite direction [20], [21].

GLT become most widely used in FI as it achieves high sensitivity, small calculation and easy implementation [22]–[24]. Lots of researchers apply KF algorithms to GLT, making GLT useful when considering errors of inertial sensors [25], [26]. However, GLT isolation approach based on KF cannot be applied to isolate a hard fault or a soft fault in four-gyro SINS.

A few researchers come up with an idea for FI—using other kinds of sensors to provide angular velocity baseline information. Fault can be isolated by checking difference between angular velocity baseline information and gyro outputs. Since 1990s, lots of domestic and foreign scholars do research on star sensors to get accurate angular velocity of a vehicle in non-gyro system, and many research results have been obtained [27]–[30]. In recent years, with the development of star sensors and the maturity of angular velocity's algorithm based on a star sensor, the accuracy of angular velocity can reach $10^{-6} rad/s$ [31], [32]. These make star sensors provide accurate angular velocity baseline information for FI. A few researchers utilize star sensors to isolate a faulty gyro. Faulty gyro can be detected and isolated through comparison between gyro outputs and angular velocity from star sensor [33], [34].This FI approach is applied in SINS, however, it cannot be used in redundant SINS when considering errors of sensors.

In this paper, with the aid of star sensors, an improved residual chi-square test fault isolation approach improves the thought of residual chi-square test, which has been widely applied to detect a fault for integrated navigation system (INS) [35], [36]. This approach first modifies the model of GLT considering the errors of inertial sensors, and redesigns a residual vector generated by gyros and star sensors for four-gyro SINS. Second, a separate residual chi-square test approach is designed to isolate a fault for each gyro. Third, to reduce soft fault isolation time, an average separate residual vector and new isolation threshold are designed. Fourth, star sensors provide accurate angular velocity baseline information to generate residual vector for FI in four-gyro SINS.

The contribution of our research are as follows. To recognize a fault in four-gyro SINS, first, a new observation model for isolation is designed. Second, separate residual chi-square test fault isolation approach is proposed to isolation a fault in four-gyro SINS. Third, average separate residual chi-square test fault isolation approach improves separate residual chi-square test approach, and reduce the isolation time of a soft fault.

The rest of this paper is organized as follows. In part II, the limitation of GLT algorithm based on KF is proved. In part III, an improved residual chi-square test fault isolation approach for four-gyro SINS is proposed. Part IV describes a redundant model, tetrahedral structure. Experimental results and discussions are presented in part V. Finally, conclusions are summarized in Part VI.

II. GLT ALGORITHM AND LIMITATION

In this part, GLT algorithm is first presented. Second, GLT algorithm based on KF is described. Third, limitation of GLT isolation algorithm is proved.

A. GLT ALGORITHM

m measurements are generated by a number of redundant inertial sensors:

$$\boldsymbol{Z} = \boldsymbol{HX} + \boldsymbol{f} + \boldsymbol{\varepsilon}, \tag{1}$$

where $\boldsymbol{Z} \in \boldsymbol{R}^m$ denotes inertial sensors' measurements. $\boldsymbol{X} \in \boldsymbol{R}^n$ is the angular velocity. $\boldsymbol{H} \in \boldsymbol{R}^{m\times n}$ is the inertial sensors' measurement matrix. $\boldsymbol{f}$ is a fault vector. $\boldsymbol{\varepsilon}$ is a measurement noise vector satisfies:

$$E(\boldsymbol{\varepsilon}) = 0, \quad E(\boldsymbol{\varepsilon}\boldsymbol{\varepsilon}^T) = \boldsymbol{R}. \tag{2}$$

A $(m-3)$-dimensional parity vector $\boldsymbol{P}$ is determined to detect and isolate a fault.

$$\boldsymbol{P} = \boldsymbol{VZ} = \boldsymbol{VHX} + \boldsymbol{Vf} + \boldsymbol{V\varepsilon}, \tag{3}$$

where $\boldsymbol{V}$ is a $(m-3)\times m$-dimensional parity matrix that satisfies

$$\boldsymbol{VV}^T = \boldsymbol{I}_{m-3}\boldsymbol{VH} = \boldsymbol{0}. \tag{4}$$

(3) can be rewritten as

$$\boldsymbol{P} = \boldsymbol{Vf} + \boldsymbol{V\varepsilon}. \tag{5}$$

The parity vector $\boldsymbol{P}$ is a vector only related to fault and noise, and $\boldsymbol{P}$ has no relationship with angular velocity.

GLT fault detection decision function is [22]:

$$FD_{GLT} = \frac{1}{\sigma^2}\left(\boldsymbol{P}^{\boldsymbol{T}}\boldsymbol{P}\right).$$
$$\text{If } FD_{\text{GLT}} \geq T_D, \text{ a fault occurs;}$$
$$\text{if } FD_{\text{GLT}} < T_D, \text{ no fault occur.} \quad (6)$$

where $FD_{GLT} \sim \chi^2(m-n)$. T_D denotes a fault detection threshold derived from Chi square distribution table according to the given false alarm rate and degree of freedom $(m-n)$.

GLT fault isolation function is shown:

$$FI_{\text{GLT}}(i) = \frac{(\boldsymbol{P}^{\text{T}}\boldsymbol{V}_i)^2}{\sigma^2\boldsymbol{V}_i^{\text{T}}\boldsymbol{V}_i}, \quad (7)$$

faulty sensor has the maximum of $FI_{\text{GLT}}(i)$. $\boldsymbol{V}_i$ is the ith column of $\boldsymbol{V}$.

B. GLT ALGORITHM BASED ON KF

In traditional GLT algorithm, the errors of sensors-input misalignment, scale factor and bias are not taken into consideration. As a result, traditional GLT algorithm cannot detect and isolate a fault. KF has been applied to compensate the errors in GLT, and makes GLT work.

When faults are not taken into consideration, (1) will be rewritten as:

$$\boldsymbol{Z} = (\boldsymbol{I} + \boldsymbol{H}_{se})[(\boldsymbol{H} + \boldsymbol{H}_{me})\boldsymbol{X} + \boldsymbol{b}_1 + \boldsymbol{\varepsilon}_1], \quad (8)$$

where $\boldsymbol{H}_{se} \in R^{m\times m}$ is a scale factor error matrix. $\boldsymbol{H}_{me} \in R^{m\times n}$ is an input misalignment error matrix. $\boldsymbol{b}_1$ is a bias vector. $\boldsymbol{\varepsilon}_1$ is Gaussian white noise with zero mean.

$$\begin{aligned}\boldsymbol{b} &= (\boldsymbol{I} + \boldsymbol{H}_{se})\boldsymbol{b}_1\\ \boldsymbol{\varepsilon} &= (\boldsymbol{I} + \boldsymbol{H}_{se})\boldsymbol{\varepsilon}_1\\ \boldsymbol{H}_m &= \boldsymbol{H} + \boldsymbol{H}_{me} + \boldsymbol{H}_{se}\boldsymbol{H}.\end{aligned} \quad (9)$$

From (3) and (4), parity vector is expressed:

$$\boldsymbol{P} = \boldsymbol{V}\boldsymbol{Z} = \boldsymbol{V}\boldsymbol{H}_m\boldsymbol{X} + \boldsymbol{V}\boldsymbol{b} + \boldsymbol{V}\boldsymbol{\varepsilon} + \boldsymbol{V}\boldsymbol{f}, \quad (10)$$

where estimation $\hat{\boldsymbol{X}}$ is:

$$\hat{\boldsymbol{X}} = (\boldsymbol{H}^{\text{T}}\boldsymbol{H})^{-1}\boldsymbol{H}^{\text{T}}\boldsymbol{Z}. \quad (11)$$

The state vector $\boldsymbol{e}$ related to $\boldsymbol{V}\boldsymbol{H}_m$ and $\boldsymbol{V}\boldsymbol{b}$ satisfies the Discrete Markov process [25]:

$$\boldsymbol{e}_k = \boldsymbol{e}_{k-1} + \boldsymbol{w}_{k-1}. \quad (12)$$

From KF, the estimation $\hat{\boldsymbol{e}}$ can be obtained.

After compensation, compensated parity vector, GLT fault detection function and isolation function based on KF are

$$\boldsymbol{P}^* = \boldsymbol{P} - \boldsymbol{V}\boldsymbol{H}_m\boldsymbol{X} - \boldsymbol{V}\boldsymbol{b} = \boldsymbol{V}\boldsymbol{\varepsilon} + \boldsymbol{V}\boldsymbol{f}. \quad (13)$$

$$FD_{\text{GLT}} = \frac{1}{\sigma^2}\left(\boldsymbol{P}^{*T}\boldsymbol{P}^*\right). \quad (14)$$

$$FI_{\text{GLT}}(i) = \frac{(\boldsymbol{P}^{*\text{T}}\boldsymbol{V}_i)^2}{\sigma^2\boldsymbol{V}_i^{\text{T}}\boldsymbol{V}_i}. \quad (15)$$

C. LIMITATION OF GLT ISOLATION BASED ON KF

GLT algorithm can only detect a fault, but fails to isolate a fault in four-gyro SINS. Here is a proof of the conclusion.

From (4) and (13), the fault vector $\boldsymbol{f}$'s projection onto the column space of $\boldsymbol{V}$ is described:

$$\hat{\boldsymbol{f}}_{null} = \boldsymbol{V}\boldsymbol{f}. \quad (16)$$

Assuming that gyro i has a fault. The fault's projection onto the column space of $\boldsymbol{V}$ is shown as $\hat{\boldsymbol{f}}_i$:

$$\hat{\boldsymbol{f}}_i = \boldsymbol{V}\boldsymbol{f}_i = \boldsymbol{V}(f\boldsymbol{e}_i) = f\boldsymbol{V}_i, \quad (17)$$

where f is the inertial sensor's fault magnitude. $\boldsymbol{e}$ is a m-dimensional column vector. The ith element of $\boldsymbol{e}_i$ is 1, and the others are 0.

According to (15), (17) can be rewritten as:

$$FI_{\text{GLT}}(i) = \frac{(\boldsymbol{P}^{*\text{T}}\boldsymbol{V}_i)^2}{\sigma^2\boldsymbol{V}_i^{\text{T}}\boldsymbol{V}_i} = \frac{f^2(\boldsymbol{V}_i^{\text{T}}\boldsymbol{V}_i)^2}{\sigma^2\boldsymbol{V}_i^{\text{T}}\boldsymbol{V}_i}. \quad (18)$$

From the property of $\boldsymbol{V}$, the rank of $\boldsymbol{V}$ is 1 in four-gyro SINS. Thus, $\boldsymbol{V}_i$ in (18) is only a scalar but not a vector. At this time, (18) is rewritten as:

$$FI_{\text{GLT}}(i) = \frac{f^2(\boldsymbol{V}_i^{\text{T}}\boldsymbol{V}_i)^2}{\sigma^2\boldsymbol{V}_i^{\text{T}}\boldsymbol{V}_i} = \frac{f^2(\boldsymbol{V}_i^{\text{T}}\boldsymbol{V}_i)}{\sigma^2} = \frac{\boldsymbol{P}^{*\text{T}}\boldsymbol{P}^*}{\sigma^2}. \quad (19)$$

From (19), no matter which inertial sensor fails in four-gyro SINS, GLT fault isolation function value will remain the same. There is no maximum value in the isolation functions. Thus, GLT isolation function based on KF cannot isolate a fault in four-gyro SINS.

From (15), GLT isolation works through judging which column of $\boldsymbol{V}$ has the same direction with the parity vector $\boldsymbol{P}^*$. Since $\boldsymbol{P}^*$ is a scalar in four-gyro SINS system, it cannot have a direction. Thus, parity vector can't be applied to isolate a fault in four-gyro SINS system either.

Simulations are conducted to verify the limitation of GLT isolation based on KF. Assuming that gyro 4 has a hard fault in the thirtieth second. The results are shown below. The gyro providing the biggest isolation value is the faulty one. Fig.1 shows that gyro 4's isolation function value is the same as others. As a result, we can't tell which gyro is faulty. The results demonstrate that fault isolation are wrong. Same situation happens when there is a soft fault in four-gyro SINS.

From these above, we can see that GLT fault isolation based on KF cannot be applied to FI in four-gyro SINS. In order to isolate a fault in four-gyro SINS, a new fault isolation approach must be designed.

III. IMPROVED RESIDUAL CHI-SQUARE TEST FAULT ISOLATION APPROACH

Improved residual chi-square test fault isolation approach, first, designs a residual vector based on KF, which is for isolating faulty gyro. Second, separate residual vector chi-square test fault isolation algorithm is proposed to isolate a fault for four-gyro SINS system. Third, average residual vector chi-square test fault isolation algorithm is designed

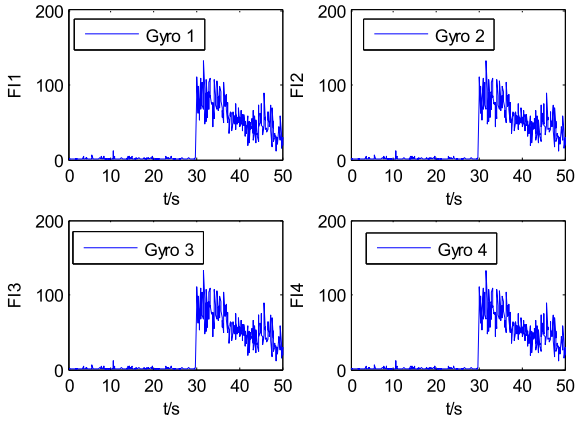

FIGURE 1. GLT fault isolation based on KF for a hard fault.

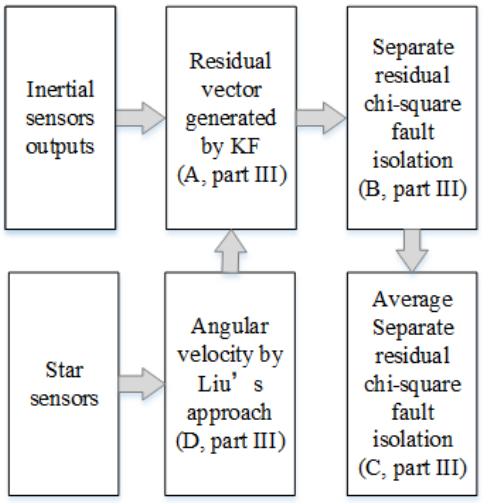

FIGURE 2. Improved residual chi-square test fault isolation approach brief flowchart.

to improve isolation performance of a soft fault. At last, an approach to obtain angular velocity of a vehicle with the aid of star sensor is presented, which can provide important observation baseline information for isolation approach.

A. RESIDUAL VECTOR BASED ON KF

In this part, first, a new isolation observation model and the state vector are designed. Second, on the basis of KF, a residual vector can be obtained through KF algorithm.

From part II, both parity vector and isolation function of GLT fail to isolate a fault in four-gyro SINS. As a result, the observation model in (10) cannot be applied to isolation anymore. A new observation model should be considered.

From (8), when there is no fault, (8) can be presented as:

$$\boldsymbol{Z} = \boldsymbol{H}\boldsymbol{X} + \boldsymbol{H}_m\boldsymbol{X} + \boldsymbol{b} + \boldsymbol{\varepsilon}. \tag{20}$$

Different from (12), $\boldsymbol{X}$ is from star sensors, and details are presented in D, part III.

From (20), there exists

$$\boldsymbol{Z} - \boldsymbol{H}\boldsymbol{X} = \boldsymbol{H}_m\boldsymbol{X} + \boldsymbol{b} + \boldsymbol{\varepsilon}. \tag{21}$$

Supposing there is a vector $\boldsymbol{q}$, and its form is presented as below:

$$\boldsymbol{q} = [q_{11} \quad q_{12} \quad q_{13} \quad q_{21} \quad \dots \quad q_{m3}]^{\mathrm{T}}, \tag{22}$$

where q_{ij} denotes $\boldsymbol{H}_m$'s element. The first part of (21) is rewritten as:

$$\boldsymbol{H}_m\boldsymbol{X} = \boldsymbol{W}\boldsymbol{q}, \tag{23}$$

where $\boldsymbol{W} \in R^{m\times 3m}$ can be denoted as:

$$\boldsymbol{W} = \begin{bmatrix} \boldsymbol{X}^{\mathrm{T}} & 000 & \dots & 000 \\ 000 & \boldsymbol{X}^{\mathrm{T}} & \dots & 000 \\ \dots & \dots & \dots & \dots \\ 000 & 000 & \dots & \boldsymbol{X}^{\mathrm{T}} \end{bmatrix}. \tag{24}$$

(21) can be expressed as:

$$\boldsymbol{Z} - \boldsymbol{H}\hat{\boldsymbol{X}} = \hat{\boldsymbol{W}}\boldsymbol{q} + \boldsymbol{b} + \boldsymbol{\varepsilon}. \tag{25}$$

A new state vector $\boldsymbol{c}$ can be extended from $\boldsymbol{q}$ and $\boldsymbol{b}$,

$$\boldsymbol{c} = \begin{bmatrix} \boldsymbol{q} \\ \boldsymbol{b} \end{bmatrix}. \tag{26}$$

Substituting (26) into (25), we can derive an observation model:

$$\boldsymbol{Z} - \boldsymbol{H}\hat{\boldsymbol{X}} = \hat{\boldsymbol{M}}\boldsymbol{c} + \boldsymbol{\varepsilon}, \tag{27}$$

where $\hat{\boldsymbol{M}} = \begin{bmatrix} \hat{\boldsymbol{W}} & \boldsymbol{I} \end{bmatrix}$.

A dynamic model is needed to get the state vector $\boldsymbol{c}$. Supposing that $\boldsymbol{c}$ can be modeled as a discrete-time Markov process [25]:

$$\boldsymbol{c}_k = \boldsymbol{\Phi}_{k|k-1}\boldsymbol{c}_{k-1} + \boldsymbol{w}_{k-1}. \tag{28}$$

where $\boldsymbol{w}_k$ denotes a white noise, and its noise covariance matrix is $\boldsymbol{Q}_k$. $\boldsymbol{\Phi}_{k|k-1}$ is a state transition matrix.

The estimation $\hat{\boldsymbol{c}}_k$ can be derived from KF:

$$\hat{\boldsymbol{c}}_{k|k-1} = \boldsymbol{\Phi}_{k|k-1}\hat{\boldsymbol{c}}_{k-1} \tag{29}$$

$$\boldsymbol{E}_{k|k-1} = \boldsymbol{\Phi}_{k|k-1}\boldsymbol{E}_{k-1}\boldsymbol{\Phi}^{T}_{k|k-1} + \boldsymbol{Q}_{k-1} \tag{30}$$

$$\boldsymbol{K}_k = \boldsymbol{E}_{k|k-1}\hat{\boldsymbol{M}}^{T}_k[\hat{\boldsymbol{M}}_k\boldsymbol{E}_{k|k-1}\hat{\boldsymbol{M}}^{T}_k + \boldsymbol{R}_k]^{-1} \tag{31}$$

$$\hat{\boldsymbol{c}}_k = \hat{\boldsymbol{c}}_{k|k-1} + \boldsymbol{K}_k[\boldsymbol{Z}_k - \boldsymbol{H}\hat{\boldsymbol{X}}_k - \hat{\boldsymbol{M}}_k\hat{\boldsymbol{c}}_{k|k-1}] \tag{32}$$

$$\boldsymbol{E}_k = [\boldsymbol{I} - \boldsymbol{K}_k\hat{\boldsymbol{M}}_k]\boldsymbol{E}_{k|k-1}. \tag{33}$$

The practical observation is

$$\boldsymbol{Z}\boldsymbol{p}_k = \boldsymbol{Z}_k - \boldsymbol{H}\hat{\boldsymbol{X}}_k, \tag{34}$$

and the predicted observation is

$$\boldsymbol{Z}\boldsymbol{p}_{k|k-1} = \hat{\boldsymbol{M}}_k\hat{\boldsymbol{c}}_{k|k-1}, \tag{35}$$

The residual vector can be contained from the difference between the practical observation outputs and the predicted observation [35]

$$\boldsymbol{r} = \boldsymbol{Z}\boldsymbol{p}_k - \boldsymbol{Z}\boldsymbol{p}_{k|k-1} = \boldsymbol{Z}_k - \boldsymbol{H}\hat{\boldsymbol{X}}_k - \hat{\boldsymbol{M}}_k\hat{\boldsymbol{c}}_{k|k-1}, \tag{36}$$

where $\boldsymbol{r}$ refers to a residual vector generated by gyros and star sensors.

B. SEPARATE RESIDUAL CHI-SQUARE TEST FAULT ISOLATION APPROACH

In traditional residual chi-square test, the function can only be used to detect a fault in INS, but it is never used to isolate a fault. In traditional residual chi-square test approach, the fault detection function [35] is

$$\lambda = \boldsymbol{r}^{\mathrm{T}} \boldsymbol{A}_k^{-1} \boldsymbol{r}, \tag{37}$$

where the residual vector $\boldsymbol{r}$ satisfies Gaussian noise with zero mean when there is no fault, and its covariance matrix is

$$\begin{aligned} \boldsymbol{A}_k &= \hat{\boldsymbol{M}}_k \boldsymbol{E}_{k|k-1} \hat{\boldsymbol{M}}_k^{\mathrm{T}} + \boldsymbol{R}_k. \\ \text{If } \lambda &\geq T_{D1}, \quad \text{there is a fault;} \\ \text{if } \lambda &< T_{D1}, \quad \text{there is no fault.} \end{aligned} \tag{38}$$

where $\lambda \sim \chi^2(m)$, as the dimension of $\boldsymbol{r}$ is m. T_{D1} denotes a fault detection threshold. It can be obtained through Chi square distribution table.

From (37), the detection function λ contains the residual information of redundant SINS. Traditional residual chi-square test approach designs a residual vector for redundant SINS. The function cannot determine which gyro has a fault. Thus, a new fault isolation approach is required to isolate a fault effectively in four-gyro SINS.

In order to achieve isolation, separate residual chi-square test fault isolation approach designs a separate residual vector for each gyro. The problem of isolation can be realized by checking whether one gyro is faulty or not. Consequently, the proposed approach can not only isolate a fault in four-gyro SINS, but also isolate a fault in any other redundant SINS.

Obviously, (36) can be rewritten as

$$\boldsymbol{r} = \boldsymbol{Z}_k - \boldsymbol{H}\hat{\boldsymbol{X}}_k - \hat{\boldsymbol{M}}_k \hat{\boldsymbol{c}}_{k|k-1} = [r_1 \quad r_2 \quad \dots \quad r_i]^{\mathrm{T}}, \tag{39}$$

where $r_i (i = 1, 2 \dots m)$ refers to a separate residual vector of gyro i.

In (39), the separate residual vector r_i satisfies Gaussian with zero mean when there is no fault, and its covariance matrix is

$$A_i = \boldsymbol{A}_k(i, i). \tag{40}$$

From (39), when there is no fault, r_i is a linear function of $\boldsymbol{\varepsilon}$. r_i is subject to 1-dimensional normal distribution. When there is a fault, the mean value of r_i is not zero. As a result, fault isolation function can be determined according to the property of r_i.

The statistical property of r_i presents differently under two situation. The normal situation is denoted as H_0, and the failure situation is denoted as H_1:

$$H_0 : E(r_i) = 0, \quad E(r_i r_i^{\mathrm{T}}) = A_i \tag{41}$$

$$H_1 : E(r_i) = f, \quad E[(r_i - f)(r_i - f)^{\mathrm{T}}] = A_i. \tag{42}$$

where f is faulty magnitude of gyro i.

A log-likelihood ratio function related to r_i is defined

$$\Lambda(r_i) = \ln \frac{P_r(r_i/H_1)}{P_r(r_i/H_0)}, \tag{43}$$

where $P_r(\cdot/\cdot)$ means normal conditional probability density function. From (43) and (44),

$$\Lambda(r_i) = \frac{1}{2}[r_i^{\mathrm{T}} r_i - (r_i - f)^{\mathrm{T}}(r_i - f)]. \tag{44}$$

From (44), the maximum likelihood estimation of f can be obtained

$$\hat{f} = r_i. \tag{45}$$

Substituting (45) into (44), we obtain (46) as follows:

$$\Lambda(r_i) = \frac{1}{2} r_i^{\mathrm{T}} r_i \tag{46}$$

Thus, separate residual chi-square test fault isolation function can be derived:

$$\begin{aligned} FR_i &= r_i^{\mathrm{T}} A_i^{-1} r_i. \\ \text{If } FR_i &\geq T_{Ii}, \quad \text{gyro } i \text{ has a fault;} \\ \text{if } FR_i &< T_{Ii}, \quad \text{gyro } i \text{ has no fault.} \end{aligned} \tag{47}$$

where $FR_i \sim \chi^2(1)$, as the dimension of r_i is 1. T_{Ii} denotes gyro i's fault isolation threshold. It can be obtained through Chi square distribution table when probability of false alarm is given.

C. AVERAGE SEPARATE RESIDUAL CHI-SQUARE TEST FAULT ISOLATION APPROACH

Separate residual chi-square test fault isolation approach can isolate a hard or a soft fault. As a soft fault can only be isolated when it accumulated to some degree, its isolation time is later than the time that the fault happens. To reduce the isolation time for a soft fault, an average separate residual chi-square test fault isolation approach is proposed.

The proposed approach can be divided into two parts: one is the proposal of an average separate residual vector, and the other is the calculation of new isolation threshold.

To decrease the influence of noise, an average separate residual vector is proposed based on the thought of weighted average. By calculating the mean value of separate residual vector through sliding data window, an average separate residual vector can be obtained.

From (39), average separate residual vector can be expressed:

$$ra_i(k) = \frac{1}{p}\left[r_i(k+1-p) + r_i(k+2-p) + \ldots + r_i(k)\right]. \tag{48}$$

From (48), (41), and (42), the statistical property of $ra_i(k)$ is:

$$H_0 : E([ra_i(k)]) = 0, E([ra_i(k)]\,[ra_i(k)]^{\mathrm{T}}) = A_i \tag{49}$$

$$H_1 : E([ra_i(k)]) = f, E[[ra_i(k) - f]\,[ra_i(k) - f]^{\mathrm{T}}] = A_i \tag{50}$$

From (47), average separate residual chi-square test fault isolation function can be obtained:

$$FRA_i(k) = ra_i(k)^{\mathrm{T}} \cdot A_i(k)^{-1} \cdot ra_i(k) \tag{51}$$

The new isolation threshold is the key to average separate residual chi-square test fault isolation. In B, part III, the isolation threshold is obtained by limiting the probability of false alarm, but it is usually too large. To get a proper isolation threshold, two steps are designed.

At the first step, the magnitude of a tolerable fault should be calculated. In redundant SINS, navigation result are calculated from three-axis inertial sensors' outputs, which are obtained by least square approach from multiple inertial sensors. The accuracy of navigation results are decided by the errors of three-axis inertial sensors' outputs. As C.K Yang said [37], if the errors of three-axis inertial sensors' outputs are the same whether there is a fault or not in redundant SINS, the fault is tolerant, and it needn't to be isolated.

When the faulty gyro is included, the error covariance $\boldsymbol{C}_{+i}$ is:

$$\boldsymbol{C}_{+i} = E[(\boldsymbol{x}_{+i} - \boldsymbol{x})(\boldsymbol{x}_{+i} - \boldsymbol{x})^{\mathrm{T}}], \tag{52}$$

where $\boldsymbol{x} = (\boldsymbol{H}^{\mathrm{T}}\boldsymbol{H})^{-1}\boldsymbol{H}^{\mathrm{T}}\boldsymbol{Z}$, $\boldsymbol{x}_{+i} = \boldsymbol{x} + (\boldsymbol{H}^{\mathrm{T}}\boldsymbol{H})^{-1}\boldsymbol{H}^{\mathrm{T}}(\boldsymbol{f} + \boldsymbol{\varepsilon})$.

When faulty gyro is not included, the error covariance $\boldsymbol{C}_{-i}$ is:

$$\boldsymbol{C}_{-i} = E[(\boldsymbol{x}_{-i} - \boldsymbol{x})(\boldsymbol{x}_{-i} - \boldsymbol{x})^{\mathrm{T}}] \tag{53}$$

where $\boldsymbol{x}_{-i} = \boldsymbol{x} + (\boldsymbol{H}^{\mathrm{T}}\boldsymbol{W}_i\boldsymbol{H})^{-1}\boldsymbol{H}^{\mathrm{T}}\boldsymbol{W}_i\boldsymbol{\varepsilon}$, and $\boldsymbol{W}_i$ is an $n \times n$ diagonal matrix with (i, i) component set to 0 and others are 1.

When (52) is equal to (53), tolerable fault can be performed (details can be found in [37]):

$$f^2 = \frac{\boldsymbol{R}}{||\boldsymbol{V}_i||^2} \tag{54}$$

Only when the magnitude of fault is bigger than tolerable fault, it can be isolated.

At the second step, new isolation threshold can be obtained from fault isolation function in (51) and tolerable fault in (54). As shown in (45), separate residual vector r_i is the maximum likelihood estimation of f. Once the tolerable fault is settled, the smallest average separate residual vector and isolation function are confirmed.

Substituting (54) into (51), new isolation threshold can be designed:

$$T_{Ri} = A_i(k)^{-1}\frac{\boldsymbol{R}}{||\boldsymbol{V}_i||^2} \tag{55}$$

where denotes gyro i's new isolation threshold.

D. ANGULAR VELOCITY ESTIMATION USING STAR SENSOR

The key to make improved fault isolation approach work is the determination of three-dimensional angular velocity $\boldsymbol{X}$ in (36). The angular velocity $\boldsymbol{X}$ provides angular motion baseline information to get residual vector in (36) and (39).

In GLT approach based on KF algorithm, angular velocity $\boldsymbol{X}$ is confirmed by the least squares estimation (LSE) of $\boldsymbol{Z}$, as (11) presented. We may find angular velocity $\boldsymbol{X}$ is used as an observation matrix in (10). When a fault occurs, the property of observation $\boldsymbol{P}$ changed. Fault can be detected through different property of $\boldsymbol{P}$. Thus, using LSE to get angular velocity $\boldsymbol{X}$ can be applied to GLT approach based on KF algorithm to detect a fault.

While in improved fault isolation approach, using LSE to get angular velocity $\boldsymbol{X}$ can't be applied. It is because angular velocity $\boldsymbol{X}$ is not only used as an observation matrix, but also as a part of the observation. From (11) and (21), once there is a fault in $\boldsymbol{Z}$, there would be faulty information in every element of observation in (21). In other words, LSE pollute every element of observation, and we can't tell which element of observation has a fault, which makes improved fault isolation cannot work. Hence, it's important to get angular velocity $\boldsymbol{X}$ without faulty information.

As we metioned in part I, a star sensor is a high accurate and autonomous sensor, which provides attitude information (or cateloged vector). Lots of researchers study how to get accurate angular velocity information based on star sensors. Among these studies, Liu proposed an adaptive Kalman Filter (AKF) to estimate angular velocity, and accuracy can reach $10^{-6} rad/s$. Thus, we can apply Liu's approach to improve the accuracy of the angular velocity. Here is the brief introduction of Liu's approach.

The measurement model of the star sensor can be considered as a pinhole imaging system. The star's direction vector is provided in the star sensor reference [32]:

$$\boldsymbol{v}(t) = \boldsymbol{M}(t)\boldsymbol{r}, \tag{56}$$

where $\boldsymbol{r}$ and $\boldsymbol{v}(t)$ represent the cataloged vector in inertial frame and the measurement direction vector in the star sensor frame, respectively. $\boldsymbol{M}(t)$ is an attitude matrix of star sensor. And $\boldsymbol{r}$ and $\boldsymbol{v}(t)$ satisfy

$$\boldsymbol{v}(t) = \frac{1}{\sqrt{x^2(t) + y^2(t) + h^2}}\begin{bmatrix} -x(t) \\ -y(t) \\ h \end{bmatrix}, \tag{57}$$

and

$$\boldsymbol{r} = \begin{bmatrix} \cos\alpha\cos\delta \\ \sin\alpha\cos\delta \\ \sin\delta \end{bmatrix}, \tag{58}$$

where α and δ are star's right ascension and declination in inertial frame, respectively. $x(t)$ and $y(t)$ are star's projection in the star sensor frame. And h represents focal distance.

The derivative with respect to t in (57)

$$\frac{\partial \boldsymbol{v}(t)}{\partial t} = \frac{\partial \boldsymbol{M}(t)}{\partial t}\boldsymbol{r} = -[\boldsymbol{X}(t)\times]\boldsymbol{M}(t)\boldsymbol{r} = [\boldsymbol{v}(t)\times]\boldsymbol{X}(t), \tag{59}$$

where $\boldsymbol{X}(t)$ is angular velocity.

The observation model and measurement model are

$$\boldsymbol{X}(t)_{k+1} = \boldsymbol{X}(t)_k + \boldsymbol{w}(t)_k \tag{60}$$

and

$$\begin{aligned} \boldsymbol{Z}_1(t)_k &= \boldsymbol{H}_1(t)_k\boldsymbol{X}(t)_k + \boldsymbol{V}(t)_k, \\ \boldsymbol{Z}_1(t)_k &= \frac{1}{\sqrt{x^2(t)_k + y^2(t)_k + h^2}}\begin{bmatrix} -x(t)_k \\ -y(t)_k \end{bmatrix} \end{aligned} \tag{61}$$

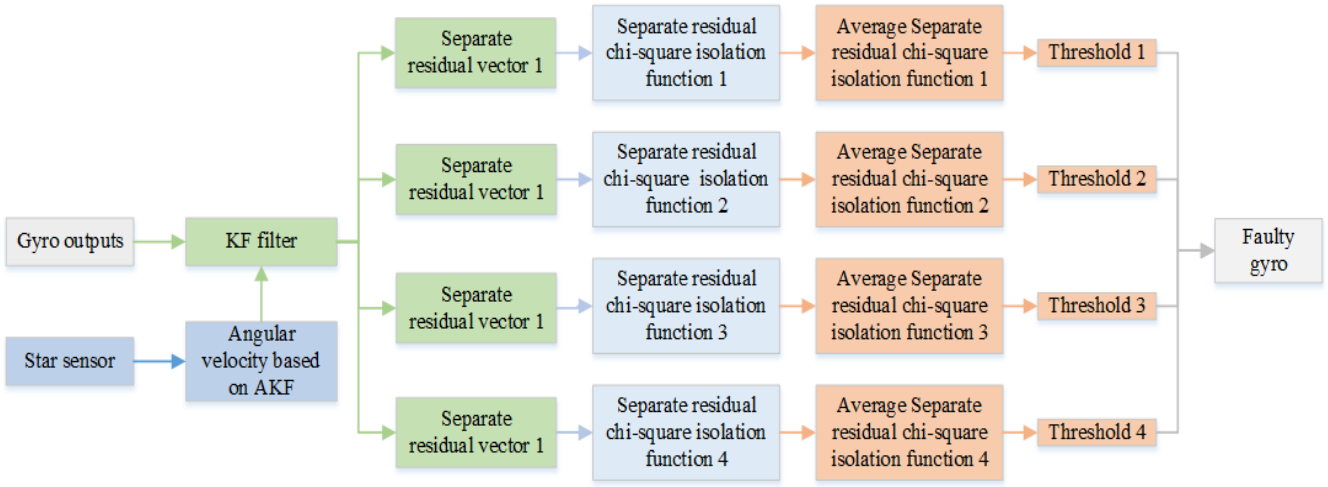

FIGURE 3. Improved residual chi-square test fault isolation approach.

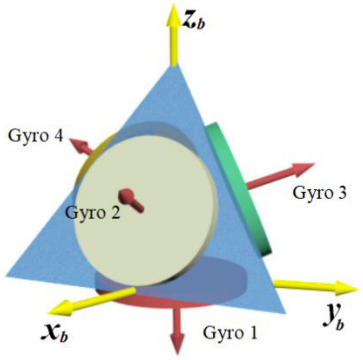

FIGURE 4. Four-gyro tetrahedral structure.

where

$$-\frac{1}{\sqrt{x^2(t)_{k-1}+y^2(t)_{k-1}+h^2}}\begin{bmatrix}-x(t)_{k-1}\\-y(t)_{k-1}\end{bmatrix}$$

and $\boldsymbol{H}_1(t)_k = \frac{1}{\sqrt{x^2(t)_k+y^2(t)_k+h^2}}\begin{bmatrix}0 & -h & y(t)_k\\ h & 0 & -x(t)_k\end{bmatrix}$.

From AKF algorithm, angular velocity $\boldsymbol{X}(t)$ can be derived.

Detailed improved residual chi-square test fault isolation approach is displayed as follows:

IV. REDUNDANT MODEL

In order to verify the proposed approach, we take four-gyro SINS as an example. Fig.4 shows a four-gyro tetrahedral structure [38]. The frame of this structure is a tetrahedron. Its bottom is a regular triangle, and its side is an isosceles triangle. The angle between bottom and side is 70.53°. The four gyros are installed on planes of the tetrahedron. In Fig.4, the axis of gyro 1 and oz_b are in opposite direction, the axis of gyro 2 is in x_boz_b plane. The angle between projection of gyro 3's axis onto x_boy_b plane and ox_b is 120°. The angle between projection of gyro 4's axis onto x_boy_b plane and ox_b is 240°.

The measurement matrix $\boldsymbol{H}$ is:

$$\boldsymbol{H} = \begin{bmatrix}0 & 0 & -1\\ 0.9428 & 0 & 0.3333\\ -0.4714 & 0.8165 & 0.3333\\ -0.4714 & -0.8165 & 0.3333\end{bmatrix}. \tag{62}$$

Compared with other redundant SINS, four-gyro tetrahedral structure's advantages are displayed:

Compared to other four-gyro SINS, a tetrahedral structure achieves greatest reliability and optimal navigation accuracy norm [39]:

$$\boldsymbol{H}^{\mathrm{T}}\boldsymbol{H} = \frac{m}{3}\boldsymbol{I}_3, \tag{63}$$

where $\boldsymbol{I}$ is equal to an identity matrix, and m denotes the number of gyros in SINS.

It is noticeable that any three of the gyros' sensitive axes are not in a plane in four-gyro tetrahedral structure. This four-gyro SINS is able to work after isolating any one of the gyros. Consequently, four-gyro tetrahedral structure is good for FI.

V. RESULTS AND DISCUSSION

A. EXPERIMENTAL CONDITION

Semi-physical simulation is conducted to test the performance of the proposed approach. Two kinds of data are needed in the experiment: the gyro outputs and star sensor outputs.

The gyros' outputs can be described as follows:

$$\hat{\boldsymbol{\omega}}_{ib}^{b} = \boldsymbol{\omega}_{ib}^{b} + \delta\boldsymbol{\omega}_{ib}^{b} \tag{64}$$

where b denotes the SINS's body frame. $\hat{\boldsymbol{\omega}}_{ib}^{b}$ represents practical angular velocity. $\delta\boldsymbol{\omega}_{ib}^{b}$ is the noise of gyro, which can be obtained from experiment in semi-physical simulation. $\boldsymbol{\omega}_{ib}^{b}$ is the true angular velocity, which is from simulation in semi-physical simulation.

In Fig.5, IMU, which is composed of three-axis gyros and three-axis accelerometers, is used for experiments. Four-gyro's noise can be obtained from two experiments.

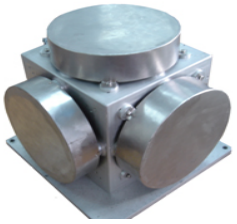

FIGURE 5. IMU of SINS.

When considering gyros' error in (8), the errors information should be considered. They are set as follows:

The scale factor error matrix is

$$\boldsymbol{H}_{se} = \begin{bmatrix} 0.005 & 0 & 0 & 0 \\ 0 & 0.005 & 0 & 0 \\ 0 & 0 & 0.005 & 0 \\ 0 & 0 & 0 & 0.005 \end{bmatrix}. \quad (65)$$

The input misalignment error matrix is given in (66), as shown at the bottom of this page, where the installation error angles are $a_1 = a_2 = b_1 = b_2 = c_1 = c_2 = d_1 = d_2 = 60''$. As bias is $0.2°/h$, the bias vector is:

$$\boldsymbol{b}_1 = [0.2 \quad 0.2 \quad 0.2 \quad 0.2 \quad 0.2 \quad 0.2]^{\mathrm{T}}. \quad (67)$$

Then gyro outputs can be confirmed considering sensor errors.

Star sensors' outputs can be modeled as follows:

$$\hat{\boldsymbol{r}}_s = \boldsymbol{r}_s + \delta \boldsymbol{r}_s. \quad (68)$$

where s denotes the star sensor's body frame. $\hat{\boldsymbol{r}}_s$ represents practical cataloged vector. $\delta \boldsymbol{r}_s$ is the noise of star sensor, which is assumed to be Gaussian white noise, and its covariance is set to be 0.1 pixels. $\boldsymbol{r}_s$ is the true cataloged vector, which is from simulation. To reduce the calculation, it's assumed that the SINS's body frame and star sensor's body frame are in the same direction. The designed focal distance is 105.75 mm. The star sensor data rate is 10 Hz.

Other detailed conditions are displayed as follows:

(1) The vehicle moves in a straight line, and the velocity is set to $6.17m/s$. The initial latitude and longitude are 45° and 126°, relatively. The resulting attitudes, pitch, roll, and heading angle of vehicle are modeled as sine functions. The amplitude/period are $9°/5s$, $8°/7\,s$ and $10°/9s$, respectively.

(2) The time of fault isolation is 50 seconds, and simulation step is 0.1 seconds.

(3) The detection threshold and isolation threshold are $T_D = T_{\mathrm{I}} = \chi^2_{0.999}(1) = 6.63$ when given false alarm rate is 0.001, and the degree of freedom is $m - n = 4 - 3 = 1$.

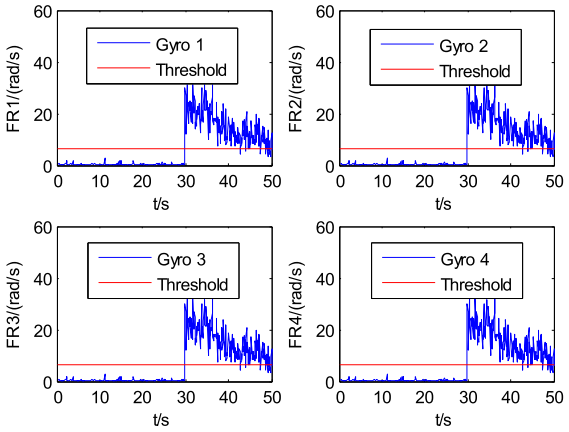

FIGURE 6. Separate residual chi-square test fault isolation for a hard fault (by LSE from gyro).

(4) A fault happens at the thirtieth second, and 2 kinds of fault conditions are shown below:

Condition A: gyro 4 has a hard fault with amplitude $10°/h$.
Condition B: gyro 4 has a soft faults with slope $1°/h$.

B. RESULT AND DISCUSSION

The proposed approach improves residual chi-square test algorithm to isolate a fault. This part first verifies the incorrectness and effectiveness of separate residual chi-square fault isolation in different condition. Second, average separate residual chi-square fault isolation is verified for four-gyro SINS in improving the isolation performance of a soft fault.

1) SEPARATE RESIDUAL CHI-SQUARE TEST FAULT ISOLATION

a: ANGULAR VELOCITY FROM GYRO

This part verifies the incorrectness of separate residual chi-square fault isolation when the angular velocity is provided by LSE from gyro. The results are shown as follows.

Separate residual chi-square test fault isolation functions in condition A are shown in Fig.6 when angular velocity is provided by LSE from gyro. Table 1 shows the detailed isolation value in Fig.6.

Separate residual chi-square test fault isolation works after GLT detect a fault in redundant SINS. The proposed approach is to determine which gyro has a fault. When a gyro's separate residual chi-square test isolation function value is bigger than isolation threshould, the gyro has a fault.

As shown in Fig.6 and table 1, gyros' isolation function values are almost the same. We cannot know which gyro is faulty. While angular velocity is calculated by LSE from

$$\boldsymbol{H} + \boldsymbol{H}_{me} = \begin{bmatrix} \sin(a_2)\cos(a_1) & \sin(a_2)\sin(a_1) & -\cos(a_2) \\ \sin(\alpha + b_2)\cos(b_1) & -\sin(\alpha + b_2)\sin(b_1) & \cos(\alpha + b_2) \\ -\sin(\alpha + c_2)\cos(c_1 + \pi - \beta) & \sin(\alpha + c_2)\sin(c_1 + \pi - \beta) & \cos(\alpha + c_2) \\ -\sin(\alpha + d_2)\cos(-d_1 + \pi - \beta) & -\sin(\alpha + d_2)\sin(-d_1 + \pi - \beta) & \cos(\alpha + d_2) \end{bmatrix} \quad (66)$$

TABLE 1. Separate residual chi-square test fault isolation for a hard fault (by lse from gyro).

Gyro \ Time	49.4	49.5	49.6	49.7	49.8	49.9	50
1	6.8991	14.5001	8.8399	8.4651	3.9316	7.2369	4.5731
2	6.8999	14.5018	8.8409	8.4661	3.9320	7.2378	4.5736
3	6.8999	14.5018	8.8409	8.4661	3.9320	7.2378	4.5736
4	6.8999	14.5018	8.8409	8.4661	3.9320	7.2378	4.5736

TABLE 2. Separate residual chi-square test fault isolation for a soft fault (by lse from gyro).

Gyro \ Time	49.4	49.5	49.6	49.7	49.8	49.9	50
1	10.4326	20.1725	25.9516	12.4676	14.9923	21.6082	12.1970
2	10.4338	20.1749	25.9547	12.4691	14.9941	21.6108	12.1985
3	10.4338	20.1749	25.9547	12.4691	14.9941	21.6108	12.1985
4	10.4338	20.1749	25.9547	12.4691	14.9941	21.6108	12.1985

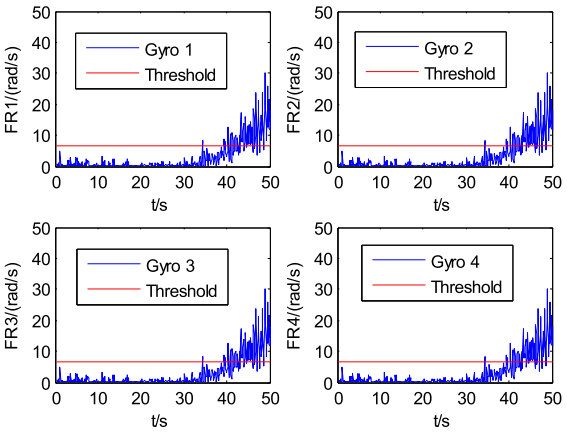

FIGURE 7. Separate residual chi-square test fault isolation for a soft fault (by LSE from gyro).

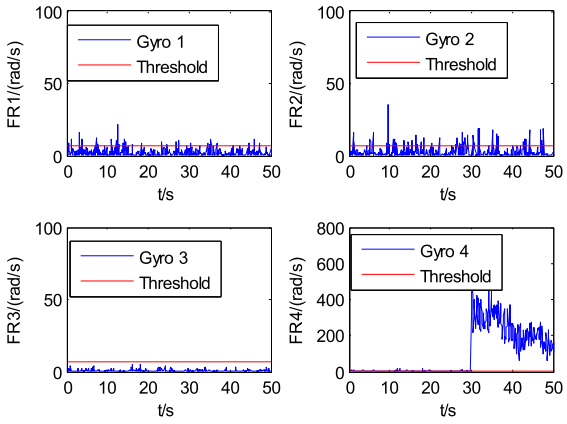

FIGURE 8. Separate residual chi-square test fault isolation for a hard fault (by AKF from star sensor).

gyro, every element of observation in (25) is polluted by some gyro's faulty information. At this time, no faulty one can be determined.

The simulation results show that when angular velocity is from gyro, separate residual chi-square test fault isolation fails to isolate a hard fault in four-gyro SINS.

Simulations are conducted for a soft fault in condition B. The results are displayed as follows. Separate residual chi-square test fault isolation functions are presented in Fig.7 when angular velocity is provided by LSE from gyro. Table 2 shows the detailed isolation value in Fig.7.

Fig.7 and table 2 show that gyros' isolation function values are nearly the same. We cannot tell which gyro has a fault. The simulation results show that separate residual chi-square test fault isolation fails to isolate a soft fault in four-gyro SINS when angular velocity is from gyro.

b: ANGULAR VELOCITY FROM STAR SENSOR

In this part, the effectiveness of separate residual chi-square test fault isolation approach is verified when angular velocity is provided by AKF from star sensor. The results are shown as follows.

Separate residual chi-square test fault isolation functions in condition A are in Fig.8 when angular velocity is provided by AKF of star sensor.

As shown in Fig.8, only gyro 4's fault isolation function value is bigger than isolation threshold. As a result, gyro 4 has a fault. Simulations show that when angular velocity is provided by star sensor, separate residual chi-square test fault isolation approach can isolate a hard fault in four-gyro SINS.

Next simulations are for soft fault in condition B. The results are presented. Separate residual chi-square test fault isolation functions in condition B are presented in Fig.9 when angular velocity is provided by AKF from star sensor.

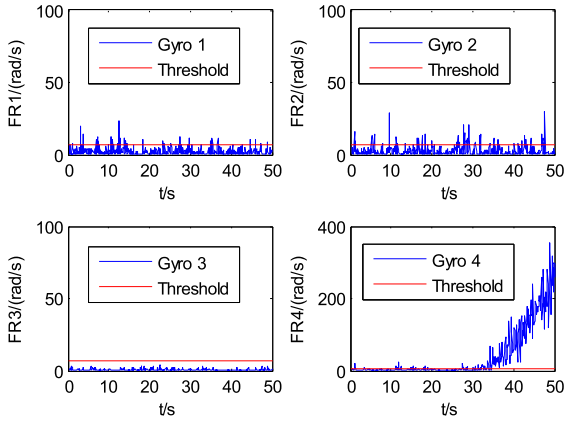

FIGURE 9. Separate residual chi-square test fault isolation for a soft fault (by AKF from star sensor).

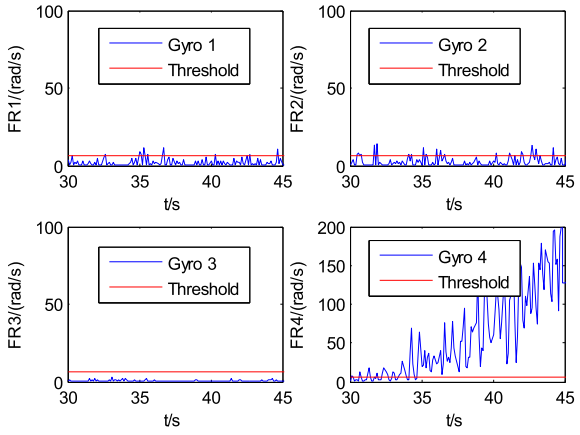

FIGURE 10. Separate residual chi-square test fault isolation for a soft fault (detailed).

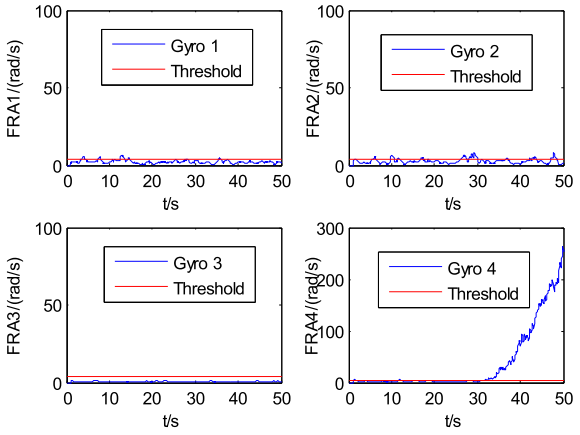

FIGURE 11. Average separate residual chi-square test fault isolation for a soft fault.

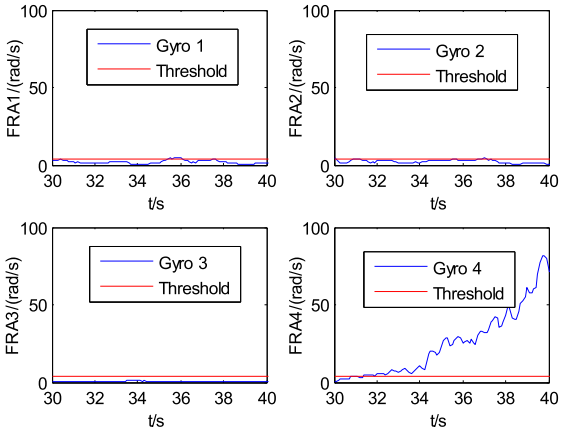

FIGURE 12. Average separate residual chi-square test fault isolation for a soft fault (detailed).

From Fig.9, gyro 4's isolation function value is much bigger than isolation threshold. We can see that gyro 4 has a soft fault. Simulations demonstrate that when angular velocity is provided by star sensor, separate residual chi-square test fault isolation approach can isolate a soft fault in four-gyro SINS.

From Fig.8, the hard fault can be isolated when the fault occurs. This approach shows good performance when there is a hard fault. However, for the soft fault in Fig.9, the fault isolation time is usually later than the time fault occurs as the soft fault always presents a slow change. Consequently, although separate residual chi-square test fault isolation approach can isolate a fault in four-gyro SINS, it cannot isolate a soft fault in time.

2) AVERAGE SEPARATE RESIDUAL CHI-SQUARE TEST FAULT ISOLATION

This part verifies the good isolation performance of average separate residual chi-square test fault isolation approach for a soft fault.

Fig.10 shows a clearer view of Fig.9. Average separate residual chi-square test fault isolation functions are presented in Fig.11. Fig.12 shows a clearer view of Fig.11.

As shown in Fig.10, when a soft fault occurs at the thirtieth second, the isolation time of gyro 4's separate residual chi-square test function is at the thirty-fifth second. In this situation, the isolation threshold is 6.63, which is obtained by checking chi-square distribution table. Obviously, separate residual chi-square test fault isolation approach cannot achieve good isolation performance for a soft isolation. From Fig.11 and Fig.12, we may find that the isolation time of gyro 4's average separate residual test function is at the thirty-second second. The new isolation threshold is 4, and it is calculated from (55). We can Obviously find that the isolation time of average separate residual chi-square test is less than that of separate residual chi-square test approach.

Comparing Fig.12 with Fig.10, on the one hand, the isolation curves in Fig.12 is much more smoother than that in Fig.10. Average separate residual chi-square test function decrease the influence of noise. On the other hand, the new threshold value is 4 in Fig.12, which is smaller than the isolation threshould (6.63) in Fig.10. Average separate residual chi-square test approach gets a proper isolation threshold for a soft fault. Thus, average separate residual chi-square test

fault isolation approach achieves good isolation peformance when a soft fault happens.

VI. CONCLUSIONS

In this paper, we propose an improved residual chi-square test fault isolation approach to solve the problem that GLT fault isolation approach based on KF cannot effectively isolate a fault in four-gyro SINS. First, the proposed approach designs a residual vector based on KF for isolation. Second, a separate residual chi-square test fault isolation approach correctly recognize a fault. Third, an average separate residual chi-square fault isolation approach reduce the soft fault isolation time. At last, a star sensor has been employed to get the angular velocity, which provides observation baseline information in the proposed isolation approach. The experimental results demonstrate that the new approach can successfully recognize a fault in four-gyro SINS.

The proposed isolation approach are designed to isolate a fault in four-gyro SINS. From part III, we may infer that the isolation approach can also isolate multiple faults in redundant SINS.

In future, more experiment should be conducted in different complex environment to verify the proposed isolation approach. Meanwhile, adaptive algorithm can be combined with the proposed isolation approach, which would improve the performance of the isolation approach in different situation.

REFERENCES

[1] G. Yan and J. Weng, *Strapdown Inertial Navigation Algorithm and Integrated Navigation Principle*. Xi'an, China: Northwestern Polytechnical Univ. Press, 2019, pp. 138–140.
[2] Y. Qin, *Inertial Navigation*. Beijing, China: Science Press, 2015, pp. 1–10.
[3] J. Cheng, P. Liu, P. Gao, M. Zou, and W. Fu, "High-precision calibration scheme for RIMU," *IEEE Access*, vol. 7, pp. 72376–72386, 2019.
[4] M. Jafari and J. Roshanian, "Inertial navigation accuracy increasing using redundant sensors," *J. Sci. Eng.*, vol. 1, no. 1, pp. 55–66, 2013.
[5] M. Jafari and J. Roshanian, "Optimal redundant sensor configuration for accuracy and reliability increasing in space inertial navigation systems," *J. Navigat.*, vol. 66, no. 2, pp. 199–208, 2012.
[6] L. Fu, X. Wang, and Y. Yue, "Method for investigation of the optimal redundant gyros number based on reliability analysis," *J. Beijing Univ. Astronaut.*, vol. 36, no. 9, pp. 1030–1033, Sep. 2010.
[7] I. Hwang, S. Kim, Y. Kim, and C. E. Seah, "A survey of fault detection, isolation, and reconfiguration methods," *IEEE Trans. Control Syst. Technol.*, vol. 18, no. 3, pp. 636–653, May 2010.
[8] S. Amir and A. Nima, "Fault detection and isolation of satellite gyroscopes using relative positions in formation flying," *Aerosp. Sci. Technol.*, vol. 78, pp. 403–417, Jul. 2018.
[9] P. Wang and R. Zhou, "Technology of fault diagnosis for dual 8-meter-configuration strapdown IMU," *Aerosp. Shanghai*, vol. 33, pp. 97–101, 2016.
[10] J. Dong, *The Research of Redundant Configuration Based on Ship Strapdown Inertial Navigation System*. Harbin, China: Harbin Engineering Univ., 2015.
[11] X. Li and H. Zhang, "Fault diagnosis and decision-making for launch vehicle SIMU with meters redundancy," *Comput. Meas. Control*, vol. 23, no. 7, pp. 2241–2243, 2015.
[12] J. Cheng, X. Sun, D. Chen, C. Cheng, H. Mou, and P. Liu, "Multi-fault detection and isolation for redundant strapdown inertial navigation system," in *Proc. IEEE/ION PLANS*, Apr. 2018, pp. 1562–1569.
[13] S. Liu, *Research on Sensors Redundant Technique of Strapdown Inertial Navigation System*. Harbin, China: Harbin Engineering Univ., 2011.
[14] Y. Luo, Q. Dai, L. Wang, and K. Wang, "INU fault diagnosis based on genetic wavelet neural network," in *Proc. 26th Chin. Control Decis. Conf.*, 2014, pp. 2837–2840.
[15] W. Wu, Z. Ren, and T. Zhang, "Improved FDI Method for a Gyro-quadruplet," *Command Control Simul.*, vol. 37, no. 1, pp. 128–131, Feb. 2015.
[16] P. Jia and H. Zhang, "Comparative research of fault detection methods based on redundant inertial measurement unit," *J. Syst. Simul.*, vol. 18, pp. 274–278, Aug. 2006.
[17] K. Xiong and H. Zhang, "Fault detection for inertial measurement unit based on local approach," *J. Beijing Univ. Astronaut.*, vol. 32, no. 7, pp. 783–787, Jul. 2006.
[18] B. Li and Z. Zhang, "Optimal parity vector technology applied to fault detection of redundant inertial measurement unit," *Aerosp. Control*, vol. 34, no. 2, pp. 86–90, Apr. 2016.
[19] H. Liang, H. Xu, and Z. Lv, "The fault diagnosis method of redundant gyroscopes based on support vector machine," *Aerosp. Control*, vol. 32, no. 5, pp. 77–83, Oct. 2014.
[20] G. Huo and J. Du, "Fault detection of strapdown inertial navigation system based on SVD," *Ship Electron. Eng.*, vol. 32, no. 1, pp. 44–45, 2012.
[21] Z. Ren, W. Fu, and T. Zhang, "New SVD method in FDI of redundant IMU," *Chin. J. Sci. Instrum.*, vol. 37, no. 2, pp. 412–419, Feb. 2016.
[22] J. Cheng, X. Sun, and H. Mou, "A modified GLT double faults isolation approach based on MLE and RPV for six-gyro redundant SINS," *IEEE Access*, vol. 7, pp. 5312–5332, 2018.
[23] L. Zhang, M. Chen, and C. Liu, "Is OPT better than GLT in fault diagnosis of redundant sensor system," *J. Northwestern Poly Tech. Univ.*, vol. 23, no. 2, pp. 266–270, Apr. 2005.
[24] Y. Wang, Z. Ren, and P. Chen, "Parity vector compensation for FDI in redundant-IMUs," *Comput. Meas. Control*, vol. 24, no. 6, pp. 34–36, Apr. 2016.
[25] Y. Wang and Z. Ren, "Parity compensation in redundant-IMUs," *Comput. Meas. Control*, vol. 24, no. 6, pp. 34–36, Feb. 2016.
[26] B. Yang, H. Pan, and X. Cai, "Study of fault detection and recognition technique in inertial redundancy system based on parity vector," *Tactical Missile Technol.*, no. 4, pp. 68–72, Apr. 2009.
[27] A. Carmi and Y. Oshman, "Fast particle filtering for attitude and angular-rate estimation from vector observations," *J. Guid., Control Dyn*, vol. 32, no. 1, pp. 70–78, 2009.
[28] T. Sun, F. Xing, and X. Wang, "An accuracy measurement method for star trackers based on direct astronomic observation," *Sci. Rep.*, vol. 6, Mar. 2016, Art. no. 22593.
[29] H. Leeghim, H. Bang, and C.-Y. Lee, "Angular rate and alignment estimation for gyroless spacecraft by only star trackers," *Int. J. Control, Automat. Syst.*, vol. 16, no. 5, pp. 2235–2243, 2018.
[30] S. Jo, H. Bang, and H. Leeghim, "A vector measurement-based angular velocity estimation scheme for maneuvering spacecraft," *J. Astron. Sci.*, vol. 64, pp. 310–332, Sep. 2017.
[31] S. Jo, Y. Chol, and H. Bang, "Optimal angular velocity estimation of spacecraft using only star tracker measurements," *J. Guid., Control Dyn*, vol. 38, no. 2, pp. 342–346, 2014.
[32] H.-B. Liu, J.-C. Yang, W.-J. Yi, J.-Q. Wang, J.-K. Yang, X.-J. Li, and J.-C. Tan, "Angular velocity estimation from measurement vectors of star tracker," *Appl. Opt.*, vol. 51, no. 16, pp. 3590–3598, Jun. 2012.
[33] Y. Zhang and P. Y. Wang, "Fault diagnosis of gyroscope based on estimated angular rate using star sensor," *Aerosp. Control*, vol. 22, no. 3, pp. 93–96, 2004.
[34] D. Hu and Y. Dong, "Gyro fault diagnosis algorithm based on vector observation," *Chin. J. Space Sci.*, vol. 31, no. 2, pp. 229–235, 2011.
[35] L. Yi-Ting, X. Xiao-Su, L. Xi-Xiang, Z. Tao, L. Yao, Y. Yi-Qing, W. Liang, and T. Jin-Wu, "A fast gradual fault detection method for underwater integrated navigation systems," *J. Navigat.*, vol. 69, no. 1, pp. 93–112, 2016.
[36] C. Zhang, X. Lu, and S. Gao, "Residual chi-square test and davar based on fault diagnosis and positioning," *Navigat. Control*, vol. 17, no. 2, pp. 25–31, Apr. 2018.
[37] C.-K. Yang and D.-S. Shim, "FDI using multiple parity vectors for redundant inertial sensors," *Eur. J. Control*, vol. 12, no. 4, pp. 437–449, 2006.
[38] J. Cheng, H. Mou, and X. Sun, "Dual-axis rotational modulation method based on sins tetrahedron redundancy configuration," *Syst. Eng. Electron.*, vol. 39, no. 8, pp. 1801–1807, Aug. 2017.
[39] D.-S. Shim and C.-K. Yang, "Optimal configuration of redundant inertial sensors for navigation and FDI performance," *Sensors*, vol. 10, no. 7, pp. 6497–6512, Jul. 2010.

JIANHUA CHENG is currently a Professor with the College of Automation, Harbin Engineering University, China. His current research interests include SINS and integrated navigation technology.

XIANGYU SUN is currently pursuing the Ph.D. degree with the College of Automation, Harbin Engineering University, China. Her current research interests include fault detection and isolation in strapdown inertial navigation systems.

PING LIU received the B.S. and M.S. degrees in electric engineering from Harbin Engineering University, Harbin, Heilongjiang, China, in 2014 and 2016, respectively. Her research interests include SINS and RIMU.

HONGJIE MOU is currently an Assistant Engineer with the Shandong Institute of Space Electronic Technology, China. His current research interest includes the development of sensor and electronic products.